

Protein Diffusion and Stokes–Einstein Deviation in Supercooled Cryoprotectant Solutions

Maddalena Bin,[†] Anita Girelli,^{†,‡} Mariia Filianina,[†] Mario Reiser,[†] Sharon Berkowicz,[†] Milla Åhlfeldt,[†] Michelle Dargasz,[¶] Sonja Timmermann,[¶] Jaqueline Savelkouls,[§] Takeshi Kawasaki,^{||,⊥} Shinji Saito,^{#,Ⓜ} Federico Zontone,[△] Yuriy Chushkin,[△] Fajun Zhang,[‡] Frank Schreiber,[‡] Michael Paulus,[▽] Christian Gutt,[¶] and Fivos Perakis*,[†]

[†]*Department of Physics, AlbaNova University Center, Stockholm University, S-106 91
Stockholm, Sweden*

[‡]*Institut für Angewandte Physik, Universität Tübingen, Auf der Morgenstelle 10, 72076
Tübingen, Germany*

[¶]*Department Physik, Universität Siegen, Walter-Flex-Strasse 3, 57072, Siegen, Germany*

[§]*Fakultät Physik/DELTA, TU Dortmund, Maria-Goeppert-Mayer-Str. 2, 44221 Dortmund,
Germany*

^{||}*D3 Center, The University of Osaka, Toyonaka, Osaka, 560-0043, Japan*

[⊥]*Department of Physics, The University of Osaka, Toyonaka, Osaka, 560-0043, Japan*

[#]*Institute for Molecular Science, Myodaiji, Okazaki, Aichi 444-8585, Japan*

[Ⓜ]*The Graduate University for Advanced Studies (SOKENDAI), Myodaiji, Okazaki, Aichi
444-8585, Japan*

[△]*ESRF - The European Synchrotron, 71 Avenue des Martyrs, Grenoble, 38000, France*

[▽]*Fakultät Physik/DELTA, TU Dortmund, 44221 Dortmund, Germany*

E-mail: f.perakis@fysik.su.se

Abstract

Vitrification during cryopreservation requires a detailed understanding of the dynamic behavior of biological solutions. We investigate ferritin diffusion in glycerol–water mixtures at supercooled temperatures using X-ray Photon Correlation Spectroscopy (XPCS). Diffusion coefficients were measured from ambient conditions to $T = 210$ K and analyzed using the Vogel–Fulcher–Tammann (VFT) relation, yielding an arrest temperature of $T_0 = 85 \pm 11$ K for ferritin ($R_h = 7.3$ nm), markedly lower than $T_0 = 122 \pm 4$ K for larger nanoparticles ($R_h = 50$ nm). Below $T \approx 230$ K, ferritin diffusion exceeds the Stokes–Einstein prediction by up to a factor of 2.7, revealing nanoscale deviations from bulk viscosity. A fluctuating–friction model quantitatively links this enhancement to local friction heterogeneity, with fluctuations increasing upon cooling and reaching $\sim 80\%$ of the mean friction at $T = 210$ K. These results establish a molecular-scale connection between protein diffusion and solvent dynamical heterogeneity in cryoprotected solutions.

Understanding protein dynamics in cryoprotected aqueous environments is central to improving cryopreservation strategies for biological and pharmaceutical systems.¹ Protein diffusion at low temperatures provides a sensitive probe of kinetically trapped and metastable states, revealing conditions that lead to denaturation or aggregation and thus determine the preservation of biological function during vitrification.

Glycerol, one of the most effective cryoprotectants, strongly influences both protein dynamics^{2,3} and structure.^{4,5} By disrupting the hydrogen-bond network of water, glycerol suppresses ice formation and extends the accessible supercooled regime.⁶ Yet, despite its widespread use, the microscopic mechanisms that govern protein motion in cryoprotected solutions under deeply supercooled conditions remain poorly understood.⁷ In particular, it is unclear how the local, heterogeneous dynamics of the solvent couple to protein diffusivity on molecular length scales.

In simple liquids, the translational diffusion coefficient $D(T)$ is often related to the solvent viscosity η by the Stokes–Einstein (SE) equation,

$$D(T) = \frac{k_B T}{6\pi\eta R_h}, \quad (1)$$

where R_h is the hydrodynamic radius and k_B the Boltzmann constant. However, a growing body of work has shown that this relation breaks down in supercooled and glass-forming liquids,^{8–12} including supercooled water¹³ and protein solutions.^{14–16} These deviations are widely attributed to the emergence of dynamical heterogeneity,¹⁷ where regions of high and low mobility coexist and evolve on nanoscopic length- and time-scales.¹⁸ Probing this coupling between protein motion and solvent heterogeneity directly remains an open challenge.

To address this challenge, we employ X-ray Photon Correlation Spectroscopy (XPCS),^{19–21} which uses coherent X-rays to probe nanoscale dynamics in complex liquids and biological systems.^{22–28} By resolving temporal correlations of the scattered X-ray intensity, XPCS directly measures collective diffusion on molecular length scales, corresponding to the mo-

momentum transfer region near the structural peak. This capability makes it ideally suited to study protein mobility in supercooled, cryoprotected solutions, where optical methods such as dynamic light scattering (DLS) are often limited by multiple scattering and opacity. Shorter time- and length-scales are typically addressed with complementary approaches using energy-resolved neutron scattering.²⁹

Here, we investigate the collective diffusion of ferritin proteins in glycerol–water mixtures from ambient to cryogenic temperatures using XPCS, complemented by small-angle X-ray scattering (SAXS) to monitor structural stability. Ferritin serves as an ideal model protein due to the high X-ray contrast from its iron core, and relevance to biomedical applications such as vaccine design³⁰ and drug delivery.³¹ By accessing momentum transfers near the structure-factor peak, we directly probe the molecular-scale dynamics that govern protein motion in supercooled cryoprotectant environments. At the low protein concentrations considered here, this diffusion corresponds to the single-particle (self) motion of ferritin rather than collective dynamics.

Figure 1 shows the small-angle X-ray scattering (SAXS) intensity $I(q)$ of ferritin in glycerol–water mixtures measured between $T = 293$ K and $T = 193$ K. The momentum transfer is defined as $q = 4\pi \sin(\theta)/\lambda$, where λ is the X-ray wavelength and 2θ the scattering angle. The data, recorded for a protein concentration of $c \approx 70$ mg mL⁻¹ (solid lines) and corrected for background scattering, display no significant change in the overall $I(q)$ profile upon cooling. The absence of major temperature-dependent changes indicates that the protein–protein interactions remain largely unchanged across the studied temperature range. Subtle variations in the intensity, on the order of 1% of the total signal, are attributed to temperature-dependent changes in the solvent compressibility.⁶ The absence of emerging peaks or intensity redistribution confirms that the ferritin structure and interparticle organization are preserved, with no evidence of cold denaturation, freezing, or nanocrystallite formation.^{5,32}

The nanoscale dynamics of the ferritin solutions were probed using XPCS.^{19–21} XPCS

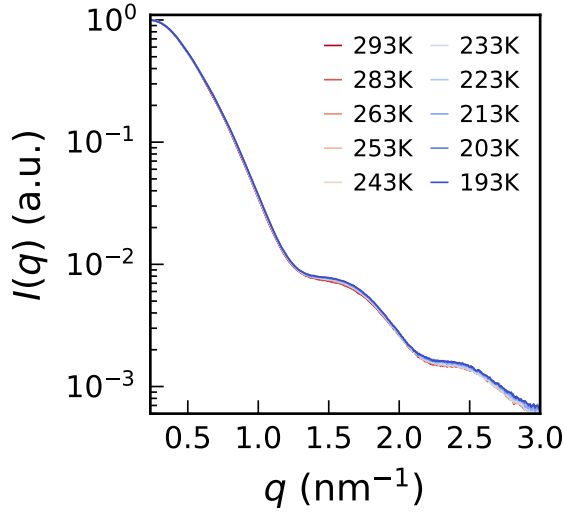


Figure 1: Temperature-dependent SAXS intensity $I(q)$ for ferritin solutions in glycerol–water mixtures at $c \approx 70 \text{ mg mL}^{-1}$ (solid lines). The nearly invariant scattering profiles indicate structural stability and the absence of cold denaturation or nanocrystallization upon cooling.

measures temporal fluctuations in the scattered X-ray intensity through the normalized intensity autocorrelation function,

$$g_2(q, t) = \frac{\langle I(q, t_0) I(q, t_0 + t) \rangle}{\langle I(q, t_0) \rangle^2}, \quad (2)$$

where $I(q, t_0)$ and $I(q, t_0 + t)$ are the intensities recorded at times t_0 and $t_0 + t$, respectively, and $\langle \dots \rangle$ denotes an average over time and detector pixels within a q -bin. The measured $g_2(q, t)$ functions were well described by a single-exponential decay,

$$g_2(q, t) = 1 + \beta \exp[-2t \Gamma(q)], \quad (3)$$

where $\Gamma(q)$ is the decorrelation rate and $\beta = 0.16$ is the speckle contrast, determined from static reference measurements. Fits using stretched exponentials yielded nearly identical relaxation times (see Supporting Information), confirming that the dynamics in this regime are dominated by diffusive relaxation.

Figure 2a shows the intensity autocorrelation functions $g_2(q, t)$ measured at $q = 0.1 \text{ nm}^{-1}$

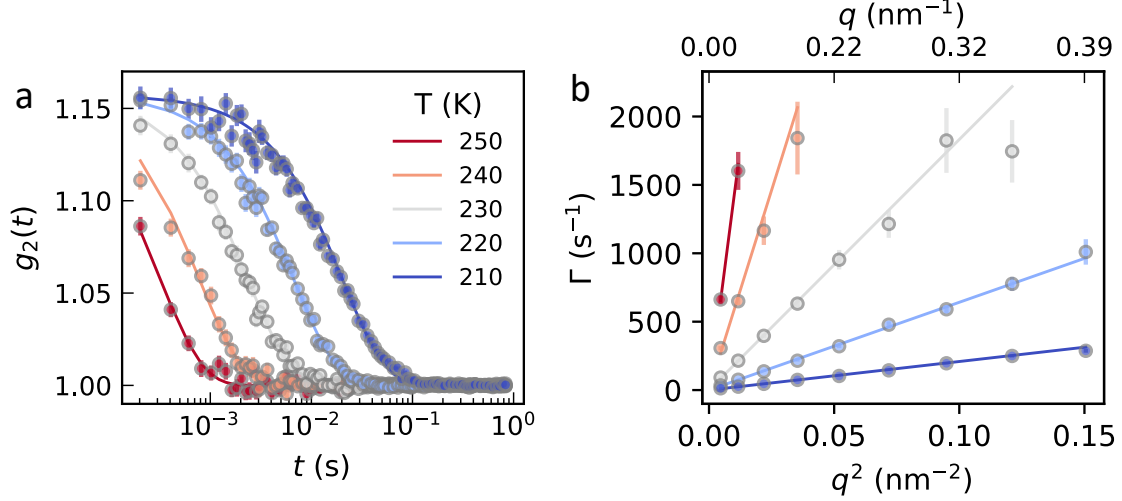


Figure 2: (a) Intensity autocorrelation functions $g_2(q, t)$ for ferritin solutions at $q = 0.1 \text{ nm}^{-1}$ and various temperatures. Solid lines represent exponential fits. (b) Relaxation rate $\Gamma(q)$ as a function of q^2 for the same temperatures. Linear fits with $\Gamma(q) = Dq^2$ yield the diffusion coefficients $D(T)$. Error bars reflect fitting uncertainties propagated from the exponential model.

for temperatures between $T = 250 \text{ K}$ and $T = 210 \text{ K}$. The decay of $g_2(q, t)$ continuously slows upon cooling, reflecting the temperature dependence of the protein dynamics. The corresponding relaxation rates $\Gamma(q)$, plotted as a function of q^2 in Fig. 2b, follow the relation $\Gamma(q) = Dq^2$, confirming purely diffusive behavior across the investigated q -range. Beam-induced effects were excluded through flux-dependent control measurements (see Supporting Information).

The extracted diffusion coefficients $D(T)$ are compared in Fig. 3a for ferritin (red triangles) and silica nanoparticle reference solutions (blue symbols) with volume fraction $\phi \approx 0.002$. The ferritin data were obtained by XPCS in the momentum-transfer range $q = 0.1 - 0.43 \text{ nm}^{-1}$, whereas the nanoparticle data were measured at $q = 0.01 - 0.05 \text{ nm}^{-1}$ and complemented by dynamic light scattering (DLS) measurements (blue squares; see Supporting Information). To account for size differences, Fig. 3b presents the diffusion coefficients normalized by the respective hydrodynamic radii, $R_h = 7.3 \text{ nm}$ for ferritin and $R_h = 50 \text{ nm}$ for the nanoparticles. We observe that the two datasets overlap down to $T = 230 \text{ K}$ and deviate below this temperature.

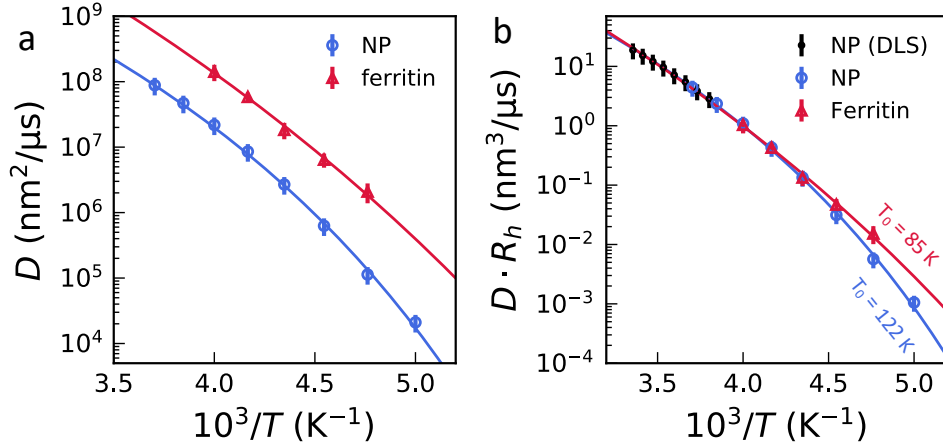


Figure 3: (a) Diffusion coefficient of ferritin solutions (red triangles) compared to nanoparticle solutions (blue circles) obtained from XPCS measurements between $T = 250 \text{ K}$ and $T = 210 \text{ K}$. Solid lines are fits using the Vogel-Fulcher-Tammann (VFT) relation. (b) The diffusion coefficients normalized by the hydrodynamics radius R_h (for ferritin $R_h = 7.3 \text{ nm}$ and for nanoparticles $R_h = 50 \text{ nm}$). Here is also shown the nanoparticle data obtained from DLS (blue squares). Solid lines are the VFT fits, where the arrest temperature T_0 is indicated.

The temperature dependence of $D(T)$ is well captured by the Vogel-Fulcher-Tammann (VFT) relation,

$$D(T) = A \exp \left[-\frac{B T_0}{T - T_0} \right], \quad (4)$$

where A is a prefactor, B relates to an apparent activation energy, and T_0 represents the dynamic arrest temperature.³³ The VFT model, which describes the non-Arrhenius slowing down of molecular motion in supercooled liquids,^{34,35} provides a good fit to both datasets. As shown in Fig. 3, the fits yield $T_0 = 122 \pm 4 \text{ K}$ for the nanoparticle solutions and $T_0 = 85 \pm 12 \text{ K}$ for the ferritin solutions. This pronounced reduction in T_0 demonstrates that proteins at the molecular scale remain mobile well below the temperature where macroscopic dynamics are effectively arrested, highlighting a strong size dependence of vitrification dynamics.

The corresponding B parameter increases from $B = 11 \pm 1$ for the nanoparticles to $B = 26 \pm 8$ for ferritin, indicating a higher apparent activation parameter for protein motion. Such behavior is consistent with the growing influence of locally slow solvent domains

at lower temperatures when their characteristic size becomes comparable to the protein radius.¹⁷ These findings emphasize that molecular-scale diffusion can differ substantially from predictions based on bulk transport properties, an important consideration for understanding vitrification in biological systems.

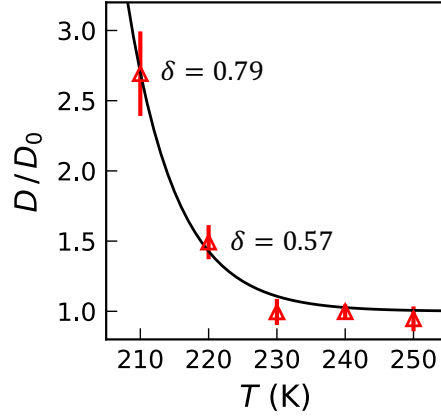


Figure 4: Ratio of the measured ferritin diffusion coefficient D to the SE-based reference D_0 (defined in Eq. 5) as a function of temperature T . The symbols show the experimental data obtained from XPCS measurements, whereas the solid line represents the prediction of the fluctuating-friction model based on Eq. 6, where $\delta = \Delta\gamma/\gamma_0$ corresponds to the relative amplitude of local friction fluctuations.

Figure 4 shows the ratio between the measured ferritin diffusion coefficient D and a Stokes–Einstein reference D_0 , defined from the nanoparticle data as

$$D_0 = \frac{R_{h,\text{NP}}}{R_{h,\text{P}}} D_{\text{NP}}, \quad (5)$$

where $R_{h,\text{P}}$ and $R_{h,\text{NP}}$ are the hydrodynamic radii of ferritin and the nanoparticles, respectively, and D_{NP} is the nanoparticle diffusion coefficient. Based on this definition, the D_0 corresponds to the diffusion coefficient that ferritin would have if it obeyed the SE relation in the same solvent environment. We assume that the nanoparticles, given the larger size and low concentration, follow the SE relation to a good approximation.³⁶ Pronounced deviations from SE behavior emerge for ferritin below $T \approx 230$ K, where D/D_0 increases up to ~ 2.7 at $T = 210$ K. We note that the nanoparticle SE relation may itself show minor deviations

at the lowest temperatures, but such effects would only reduce the apparent SE violation for ferritin and therefore cannot account for the large enhancement observed. Variations in hydrodynamic boundary conditions, from stick to slip, could alter the SE prefactor from 6 to 4,¹⁵ yet such a change is insufficient to explain the observed enhancement, indicating a genuine breakdown of the SE relation at the molecular scale.

The measured deviations highlight that diffusion probed at momentum transfers corresponding to protein length scales does not simply reflect macroscopic transport governed by the bulk viscosity. Instead, the results point to the coupling of protein motion to spatially heterogeneous solvent dynamics, where regions of high and low mobility coexist in the super-cooled state. Upon cooling, these dynamically heterogeneous domains are known to grow in both size and lifetime; for glycerol–water mixtures, slow domains can extend to ~ 10 nm,³⁷ approaching the hydrodynamic radius of ferritin ($R_h = 7.3$ nm). These domains can be ascribed to glycerol-rich and glycerol-poor patches that develop upon cooling, corresponding to nanoregions with different local viscosity.³⁸ Because the diffusion coefficient scales inversely with the local friction, $D \propto 1/\gamma$, motion in the low-viscosity regions contributes disproportionately to the mean-square displacement; as a result, the effective diffusion can exceed the SE estimate based on the average viscosity, leading to the observed SE violation.³⁹

The observed temperature dependence motivates a closer examination of how local viscosity fluctuations influence molecular diffusion. To explore the mechanism underlying the SE deviation, we employ a minimal model in which the local friction experienced by the protein is not constant but fluctuates due to temporal and spatial heterogeneities in the surrounding solvent. Following the framework in Ref.⁴⁰ the instantaneous friction coefficient $\gamma(t)$ is expressed as $\gamma(t) = \gamma_0 + \Delta\gamma(t)$, where γ_0 is the average (macroscopic) friction coefficient and $\Delta\gamma(t)$ represents the fluctuations around this mean. The average friction γ_0 is related to the macroscopic viscosity η through the Stokes relation $\gamma_0 = 6\pi\eta R_h$, which defines the corresponding SE diffusion coefficient $D_0 = k_B T / \gamma_0$. The parameter $\Delta\gamma$ quantifies the local deviations of the instantaneous friction from its mean value and can be expressed in di-

mensionless form as $\delta = \Delta\gamma/\gamma_0$. In the fast-fluctuation limit of $\Delta\gamma(t)$, the protein effectively experiences the average friction coefficient, and its diffusion coefficient can be expressed as D_0 . In contrast, in the slow-fluctuation limit, where the protein motion averages over quasi-static domains of different local viscosity, the effective diffusion coefficient is given by (Eq. 43 in Ref.⁴⁰)

$$\frac{D}{D_0} = \frac{1}{1 - \delta^2}. \quad (6)$$

This relation links the observed enhancement of D/D_0 directly to the magnitude of local friction heterogeneity, providing a quantitative measure of the amplitude of dynamical fluctuations in the solvent. At $T = 220$ K, the extracted value is $\delta \approx 0.57$, while at $T = 210$ K it increases to $\delta \approx 0.79$, indicates that the local friction deviates by nearly $\sim 80\%$ from its mean, consistent with the progressive enhancement of spatial heterogeneity upon cooling.

In summary, by combining XPCS and SAXS, we resolve nanoscale dynamics of ferritin proteins in glycerol–water solutions across the supercooled regime. This approach closes a critical gap in understanding protein motion in cryoprotected environments and demonstrates that XPCS can directly access molecular diffusion at cryogenic temperatures. The SAXS data confirm that the structural integrity of ferritin is preserved throughout the temperature range, with no indication of cold denaturation or nanocrystallite formation, while XPCS reveals a pronounced deviation from SE behavior below $T \approx 230$ K.

Analysis with the Vogel–Fulcher–Tammann (VFT) relation shows that ferritin diffusion exhibits a substantially lower dynamic arrest temperature ($T_0 = 85 \pm 11$ K) and a higher apparent activation parameter ($B = 26 \pm 8$) compared with nanoparticle solutions (with $T_0 = 122 \pm 4$ K and $B = 11 \pm 1$). This size dependence and SE breakdown reflect the coupling of protein motion to the solvent’s dynamical heterogeneity, which becomes increasingly pronounced as the correlation length of slow domains approaches the protein size.¹⁷ To quantify this effect, we employed a minimal fluctuating–friction model in which the instantaneous friction coefficient $\gamma(t) = \gamma_0 + \Delta\gamma(t)$ fluctuates around its mean due to local viscosity variations. The model links the observed enhancement in D/D_0 to the relative

amplitude of these fluctuations, $\delta = \Delta\gamma/\gamma_0$, revealing that δ increases sharply upon cooling below 230 K and reaches nearly $\sim 80\%$ of the mean friction at 210 K. This quantity provides a direct quantitative measure of the growing local friction heterogeneity in the supercooled state.

These findings offer molecular-level insight into how proteins experience vitrification in glycerol–water cryoprotectant mixtures. While conventional cryopreservation protocols rely on macroscopic glass transition temperatures, our results demonstrate that protein molecules can remain mobile far below the apparent T_g of the solvent, which for the current glycerol–water concentration is $T_g \approx 165$ K. This highlights the need to consider the coupling between solute dynamics and solvent heterogeneity when optimizing cryoprotectant formulations and vitrification strategies for biological systems.

Methods

Ferritin solutions were prepared from equine spleen ferritin (Sigma–Aldrich, F4503) at an initial protein concentration of $c = 71 \text{ mg mL}^{-1}$ in 150 mM NaCl. The stock solution was concentrated by centrifugation for 1 h at 10,000 g using 10 kDa Millipore filters, yielding a ferritin concentration of approximately $c = 730 \text{ mg mL}^{-1}$. This concentrated solution was then diluted with glycerol and water to obtain intermediate protein concentrations of $c = 70 \pm 40 \text{ mg mL}^{-1}$ (used for the SAXS measurements) and $c = 100 \pm 40 \text{ mg mL}^{-1}$ (used for XPCS measurements) in glycerol–water mixtures with a 23 mol% glycerol fraction. At these conditions, the protein volume fraction was $\phi = 0.047$, and the hydrodynamic ratio $h = R_h/R_p = 0.075$, using $R_h = 7.3 \text{ nm}$ (measured by DLS, see Supporting Information) and $R_p = 6.25 \text{ nm}$ from structural data.⁴¹ For comparison, silica nanoparticle suspensions were prepared in the same glycerol–water mixture (23 mol% glycerol) at a particle volume fraction of $\phi \approx 0.002$.

SAXS experiments were performed at beamline BL2 of the Dortmund Synchrotron Radiation

Table 1: Experimental parameters for XPCS (ESRF-ID10) and SAXS (DELTA-BL2) measurements.

Parameter	ESRF-ID10	DELTA-BL2
Photon energy (keV)	9	12
Beam size	$25 \times 25 \mu\text{m}^2$	$0.6 \times 0.6 \text{ mm}^2$
Flux (ph/s)	7×10^{10}	1.7×10^9
Detector	Eiger 500k	MAR345
Sample-detector distance (m)	7.11	1.659

Source DELTA⁴² using 12 keV photons and a sample-detector distance of 1.659 m. XPCS measurements were carried out at the ID10 beamline of the European Synchrotron Radiation Facility (ESRF, proposal SC-5375), using coherent 9 keV X-rays in SAXS geometry with an Eiger 500k detector positioned 7.11 m from the sample. This configuration provided access to a momentum-transfer range of $q = 0.10\text{--}0.43 \text{ nm}^{-1}$. The incident beam had a full-width at half-maximum of $25 \times 25 \mu\text{m}^2$ and a flux of $7 \times 10^{10} \text{ ph s}^{-1}$. Samples were loaded into 1.5 mm diameter quartz capillaries and mounted in a nitrogen gas cryostat,⁴³ allowing temperature control down to $T = 200 \text{ K}$. To minimize beam-induced effects, the sample position was refreshed for each exposure. For each temperature, approximately 120 positions were recorded per capillary with $60 \mu\text{m}$ spacing, ensuring sufficient statistics and signal-to-noise.

Acknowledgement

We acknowledge the European Synchrotron Radiation Facility (ESRF) for provision of synchrotron radiation facilities at ID10 beamline (proposal number SC-5275 and SC-5359) and would like to thank the staff for their assistance. We also thank the DELTA machine group for providing synchrotron radiation for sample characterization. FP acknowledges financial support by the Swedish National Research Council (Vetenskapsrådet) under Grant No. 2019-05542, 2023-05339 and within the Röntgen-Ångström Cluster Grant No. 2019-06075, and the kind financial support from Knut och Alice Wallenberg foundation (WAF, Grant.

No. 2023.0052). This research is supported by the Center of Molecular Water Science (CMWS) of DESY in an Early Science Project, the MaxWater initiative of the Max-Planck-Gesellschaft, Carl Tryggers (Project No. CTS21:1589) and the Wenner-Gren Foundations (Project No. UPD2021-0144). F.P. and A.G. acknowledge funding from the European Union’s Horizon Europe research and innovation program under the Marie Skłodowska-Curie grant agreement No. 101149230 (CRYSTAL-X). We also acknowledge BMBR ErUM-Pro funding (05K22PS1, CG), BMBF (05K19PS1 and 05K20PSA, CG; 05K19VTB, FS and FZ), DFG-ANR (SCHR700/28-1, SCHR700/42-1, FS and FZ). CG and FS acknowledge financial support by the consortium DAPHNE4NFDI in association with the German National Research Data Infrastructure (NFDI) e.V. - project number 46024879. SS acknowledges financial support by JSPS through the Grant-in-Aid for Scientific Research (JP21H04676 and JP23K17361). TK acknowledges support by the JST FOREST Program (Grant No. JPMJFR212T), AMED Moonshot Program (Grant No. JP22zf0127009), JSPS KAKENHI (Grant No. JP24H02203), and Takeda Science Foundation.

References

- (1) Murray, K. A.; Gibson, M. I. Chemical approaches to cryopreservation. *Nat. Rev. Chem.* **2022**, *6*, 579–593.
- (2) Caliskan, G.; Kisliuk, A.; Tsai, A. M.; Soles, C. L.; Sokolov, A. P. Protein dynamics in viscous solvents. *J. Chem. Phys.* **2003**, *118*, 4230–4236.
- (3) Dirama, T. E.; Carri, G. A.; Sokolov, A. P. Coupling between lysozyme and glycerol dynamics: Microscopic insights from molecular-dynamics simulations. *J. Chem. Phys.* **2005**, *122*, 244910.
- (4) Hirai, M.; Ajito, S.; Sugiyama, M.; Iwase, H.; Takata, S.-i.; Shimizu, N.; Igarashi, N.;

- Martel, A.; Porcar, L. Direct Evidence for the Effect of Glycerol on Protein Hydration and Thermal Structural Transition. *Biophys. J.* **2018**, *115*, 313–327.
- (5) Filianina, M.; Bin, M.; Berkowicz, S.; Reiser, M.; Li, H.; Timmermann, S.; Blankenburg, M.; Amann-Winkel, K.; Gutt, C.; Perakis, F. Nanocrystallites Modulate Inter-molecular Interactions in Cryoprotected Protein Solutions. *J. Phys. Chem. B* **2023**, *127*, 6197–6204.
 - (6) Berkowicz, S.; Andronis, I.; Girelli, A.; Filianina, M.; Bin, M.; Nam, K.; Shin, M.; Kowalewski, M.; Katayama, T.; Giovambattista, N.; Kim, K. H.; Perakis, F. Super-critical density fluctuations and structural heterogeneity in supercooled water-glycerol microdroplets. *Nat. Commun.* **2024**, *15*, 10610.
 - (7) Zaragoza, A.; Kumar, R.; Martin Roca, J.; Khatua, P.; Molinero, V.; Caupin, F.; Valeriani, C. Anomalous Behaviour of Transport Properties in a Supercooled Water–Glycerol Mixture. *Mol. Phys.* **2024**, *122*, e2413925.
 - (8) Charbonneau, P.; Jin, Y.; Parisi, G.; Zamponi, F. Hopping and the Stokes–Einstein relation breakdown in simple glass formers. *Proc. Natl. Acad. Sci. U.S.A.* **2014**, *111*, 15025–15030.
 - (9) Sengupta, S.; Karmakar, S.; Dasgupta, C.; Sastry, S. Breakdown of the Stokes-Einstein relation in two, three, and four dimensions. *J. Chem. Phys.* **2013**, *138*, 12A548.
 - (10) Das, P.; Sastry, S. Crossover in dynamics in the Kob-Andersen binary mixture glass-forming liquid. *J. Non-Cryst. Solids: X* **2022**, *14*, 100098.
 - (11) Hodgdon, J. A.; Stillinger, F. H. Stokes-Einstein violation in glass-forming liquids. *Phys. Rev. E* **1993**, *48*, 207–213.
 - (12) Mallamace, F.; Corsaro, C.; Mallamace, D.; Vasi, S.; Vasi, C.; Stanley, H. E. Some

- considerations on the transport properties of water-glycerol suspensions. *J. Chem. Phys.* **2016**, *144*, 014501.
- (13) Kawasaki, T.; Kim, K. Identifying time scales for violation/preservation of Stokes-Einstein relation in supercooled water. *Sci. Adv.* **2017**, *3*, e1700399.
 - (14) Lamanna, R.; Delmelle, M.; Cannistraro, S. Solvent Stokes-Einstein violation in aqueous protein solutions. *Phys. Rev. E* **1994**, *49*, 5878–5880.
 - (15) Chirico, G.; Placidi, M.; Cannistraro, S. Fractional Stokes-Einstein Relationship in Biological Colloids: Role of Mixed Stick-Slip Boundary Conditions. *J. Phys. Chem. B* **1999**, *103*, 1746–1751.
 - (16) Joshi, K.; Bhuyan, A. K. Glycerol-slaved 1H-1H NMR cross-relaxation in quasi-native lysozyme. *Biophys. Chem.* **2024**, *312*, 107286.
 - (17) Ediger, M. D. Spatially Heterogeneous Dynamics in Supercooled Liquids. *Annu. Rev. Phys. Chem.* **2000**, *51*, 99–128.
 - (18) Becker, S. R.; Poole, P. H.; Starr, F. W. Fractional Stokes-Einstein and Debye-Stokes-Einstein Relations in a Network-Forming Liquid. *Phys. Rev. Lett.* **2006**, *97*, 055901.
 - (19) Madsen, A.; Fluerasu, A.; Ruta, B. In *Synchrotron Light Sources and Free-Electron Lasers: Accelerator Physics, Instrumentation and Science Applications*; Jaeschke, E. J., Khan, S., Schneider, J. R., Hastings, J. B., Eds.; 2016; pp 1617–1641.
 - (20) Möller, J.; Sprung, M.; Madsen, A.; Gutt, C. X-ray photon correlation spectroscopy of protein dynamics at nearly diffraction-limited storage rings. *IUCrJ* **2019**, *6*, 794–803.
 - (21) Perakis, F.; Gutt, C. Towards molecular movies with X-ray photon correlation spectroscopy. *Phys. Chem. Chem. Phys.* **2020**, *22*, 19443–19453.
 - (22) Reiser, M. et al. Resolving molecular diffusion and aggregation of antibody proteins with megahertz X-ray free-electron laser pulses. *Nat. Commun.* **2022**, *13*, 1–10.

- (23) Girelli, A.; Rahmann, H.; Begam, N.; Ragulskaya, A.; Reiser, M.; Chandran, S.; Westermeier, F.; Sprung, M.; Zhang, F.; Gutt, C.; Schreiber, F. Microscopic Dynamics of Liquid-Liquid Phase Separation and Domain Coarsening in a Protein Solution Revealed by X-Ray Photon Correlation Spectroscopy. *Phys. Rev. Lett.* **2021**, *126*, 138004.
- (24) Begam, N.; Ragulskaya, A.; Girelli, A.; Rahmann, H.; Chandran, S.; Westermeier, F.; Reiser, M.; Sprung, M.; Zhang, F.; Gutt, C.; Schreiber, F. Kinetics of network formation and heterogeneous dynamics of an egg white gel revealed by coherent X-Ray scattering. *Phys. Rev. Lett.* **2021**, *126*, 098001.
- (25) Timmermann, S. et al. X-ray driven and intrinsic dynamics in protein gels. *Sci. Rep.* **2023**, *13*, 11048.
- (26) Chushkin, Y.; Gulotta, A.; Roosen-Runge, F.; Pal, A.; Stradner, A.; Schurtenberger, P. Probing Cage Relaxation in Concentrated Protein Solutions by X-Ray Photon Correlation Spectroscopy. *Phys. Rev. Lett.* **2022**, *129*, 238001.
- (27) Ragulskaya, A.; Begam, N.; Girelli, A.; Rahmann, H.; Reiser, M.; Westermeier, F.; Sprung, M.; Zhang, F.; Gutt, C.; Schreiber, F. Interplay between Kinetics and Dynamics of Liquid-Liquid Phase Separation in a Protein Solution Revealed by Coherent X-ray Spectroscopy. *J. Phys. Chem. Lett.* **2021**, *12*, 7085–7090.
- (28) Anthuparambil, N. D. et al. Exploring non-equilibrium processes and spatio-temporal scaling laws in heated egg yolk using coherent X-rays. *Nat. Commun.* **2023**, *14*, 5580.
- (29) Grimaldo, M.; Roosen-Runge, F.; Zhang, F.; Schreiber, F.; Seydel, T. Dynamics of proteins in solution. *Q. Rev. Biophys.* **2019**, *52*.
- (30) Rodrigues, M. Q.; Alves, P. M.; Roldão, A. Functionalizing Ferritin Nanoparticles for Vaccine Development. *Pharmaceutics* **2021**, *13*, 1621.

- (31) Zhu, Y.; Zhu, Y.; Cao, T.; Liu, X.; Liu, X.; Yan, Y.; Shi, Y.; Wang, J.-C. Ferritin-based nanomedicine for disease treatment. *Med. Rev.* **2021**, *3*, 49–74.
- (32) Boutet, S.; Robinson, I. K. Precrystallization clusters of holoferritin and apoferritin at low temperature. *Phys. Rev. E* **2007**, *75*.
- (33) Chen, B.; Sigmund, E. E.; Halperin, W. P. Stokes-Einstein Relation in Supercooled Aqueous Solutions of Glycerol. *Phys. Rev. Lett.* **2006**, *96*, 145502.
- (34) Angell, C. A. Relaxation in liquids, polymers and plastic crystals — strong/fragile patterns and problems. *J. Non-Cryst. Solids* **1991**, *131-133*, 13–31.
- (35) Turnbull, D.; Cohen, M. H. Free-Volume Model of the Amorphous Phase: Glass Transition. *J. Chem. Phys.* **1961**, *34*, 120–125.
- (36) Berkowicz, S.; Perakis, F. Exploring the Validity of the Stokes-Einstein Relation in Supercooled Water Using Nanomolecular Probes. *Phys. Chem. Chem. Phys.* **2021**,
- (37) Murata, K.-i.; Tanaka, H. Liquid–liquid transition without macroscopic phase separation in a water–glycerol mixture. *Nat. Mater.* **2012**, *11*, 436–443.
- (38) Bachler, J.; Fuentes-Landete, V.; A. Jahn, D.; Wong, J.; Giovambattista, N.; Loerting, T. Glass Polymorphism in Glycerol–Water Mixtures: II. Experimental Studies. *Phys. Chem. Chem. Phys.* **2016**, *18*, 11058–11068.
- (39) Tuteja, A.; Mackay, M. E.; Narayanan, S.; Asokan, S.; Wong, M. S. Breakdown of the Continuum Stokes-Einstein Relation for Nanoparticle Diffusion. *Nano Lett.* **2007**, *7*, 1276–1281.
- (40) Rozenfeld, R.; Luczka, J.; Talkner, P. Brownian motion in a fluctuating medium. *Phys. Lett. A* **1998**, *249*, 409–414.
- (41) Harrison, P. M. The structure and function of ferritin. *Biochem. Educ.* **1986**, *14*, 154–162.

- (42) Dargasz, M.; Bolle, J.; Faulstich, A.; Schneider, E.; Kowalski, M.; Sternemann, C.; Savelkouls, J.; Murphy, B.; Paulus, M. X-ray scattering at beamline BL2 of DELTA: Studies of lysozyme-lysozyme interaction in heavy water and structure formation in 1-hexanol. *J. Phys. Conf. Ser.* **2022**, *2380*, 012031.
- (43) Steinmann, R.; Chushkin, Y.; Caronna, C.; Chavanne, J.; Madsen, A. A small-angle scattering chamber for x-ray photon correlation spectroscopy at low temperatures. *Rev. Sci. Instrum.* **2011**, *82*, 025109.